Low mobility of CuO and TiO2 nanoparticles in agricultural soils of contrasting texture and organic matter content

Marie Simonin, Jean M.F. Martins, Gaëlle Uzu, Lorenzo Spadini, Aline Navel, Agnes Richaume

Low mobility of CuO and TiO_2 nanoparticles in agricultural soils of contrasting texture and organic matter content

Marie SIMONIN[1,2, †], Jean M. F. MARTINS[1*], Gaëlle UZU[1], Lorenzo SPADINI[1], Aline NAVEL[1], and Agnès RICHAUME[2]

[1] Univ. Grenoble Alpes, CNRS, G-INP, IRD, IGE, F-38000 Grenoble, France

[2] Univ. Lyon, Université Claude Bernard Lyon 1, CNRS, INRAE, VetAgro Sup, UMR Ecologie Microbienne, F 69622 Villeurbanne, France

[*]Correspondence to: jean.martins@univ-grenoble-alpes.fr

† Present address: IRHS-UMR1345, Université d'Angers, INRAE, Institut Agro, SFR 4207 QuaSaV, 49071, Beaucouzé, France

ABSTRACT

The fate of nanoparticles (NPs) in soil under relevant environmental conditions is still poorly understood. In this study, the mobility of two metal-oxide nanoparticles (CuO and TiO_2) in contrasting agricultural soils was investigated in water-saturated soil columns. The transport of TiO_2 and CuO-NPs were assessed in six soils with three different textures (from sand to clay) and two contrasted organic matter (OM) contents for each texture. TiO_2 mobility was very low in all soils, regardless of texture and OM content. Mass recoveries were always less than 5%, probably in relation with the strong homo-aggregation of TiO_2-NPs observed in all soil solutions, with apparent sizes 3-6 times larger than their nominal size. This low mobility suggests that TiO_2-NPs present a low risk of direct groundwater contamination in contrasted surface soils. Although their retention was also generally high (more than 86%), CuO nanoparticles were found to be mobile in all soils. This is probably related to their smaller apparent size and low capacity of homo-aggregation of CuO-NPs in all soil solutions. No clear influence of neither soil texture or soil total organic matter content could be observed on CuO transport. However, this study shows that in contrasted agricultural soils, CuO-NPs transport is mainly controlled by the solutes dissolved in soil solution (DOC and PO_4 species), rather than by the properties of the soil solid phase.

Keywords: Contrasted soils, Nanomaterials, Transfer, Dissolved organic carbon, CDE modelling, Nanoparticles' fate.

Highlights:

- Limited mobility of CuO and TiO_2 nanoparticles in contrasted agricultural soils
- DOM and dissolved P species appear as drivers of soil CuO NPs mobility
- Lower mobility of TiO_2 nanoparticles than CuO likely due to higher homoaggregation

Introduction

Metal oxide engineered nanoparticles (NPs) are now integral elements of a myriad of consumer and industrial products. Copper oxide (CuO) NPs are widely used in catalysts, superconductors or paints for their biocidal properties (Zhu *et al.* 2004; Ren *et al.* 2009; Keller *et al.* 2013). Titanium dioxide (TiO_2) NPs are commonly incorporated in personal care products, paints or food packaging (Keller *et al.* 2013). As a result, soils are exposed to these components through various exposure routes, which may result in potential risks to human and ecosystems health. Their release into soils can occur during industrial production, landfills, agricultural amendments of sewage sludge, abrasion of materials and accidental spill (Nowack *et al.* 2012). Thus, there appears to be an urgent need to improve our current knowledge of the fate and transport of NPs in soils in order to better assess the risks for groundwater and agricultural soils. Transport of NPs has been extensively investigated in poorly-reactive and well-defined porous media, such as glass beads or quartz sand, but only a few investigations have addressed the transport of metallic NPs in natural soils (e.g. Fang *et al.* 2009, 2011; Cornelis *et al.* 2013; Braun *et al.* 2015; Simonin *et al.* 2016). Soils are porous systems consisting of complex structured assemblages of mineral and organic particles combined with liquid and gaseous phases (Spadini *et al.* 2018). Several soil components such as clay and organic matter (OM) are known to influence the mobility of various pollutants or colloids due to their large reactive surfaces, which can interact with them, thus modifying their physicochemical behavior (Pan and Xing 2012). Some studies have demonstrated the influence of these factors on the aggregation, surface charge and stability of NPs (Fang *et al.* 2009; Thio *et al.* 2011; Zhou *et al.* 2012). Dissolved OM is known to promote NPs dispersion and potentially their mobility in simple porous media (Ben-Moshe, Dror and Berkowitz 2010; Thio, Zhou and Keller 2011; Simonin *et al.* 2015), while clay particles can destabilize positively and negatively charged NPs and thus decrease their mobility (Zhou *et al.* 2012). In addition, these processes are strongly

influenced by the chemistry of soil solution, such as pH, ionic strength and electrolytes such as inorganic ions (Wang *et al.* 2012; Cornelis *et al.* 2014; Vitorge *et al.* 2014). Fang *et al.* (2011) demonstrated that TiO_2-NPs could act as a metal carrier and facilitate for instance the mobilization of metals, such as copper, in soil. These results raise concerns about the potential environmental risk associated with increased migration rates of co-contaminants and increased bioavailability of some toxic metals in the presence of NPs (Chekli *et al.* 2016; Fang *et al.* 2016). Because of the interactions between these multiple environmental factors in natural soils, it is difficult to predict the fate of NPs in soil based on investigations conducted in simple and poorly reactive porous media. In particular, it remains very difficult to hierarchize the dominant factors controlling the transfer of manufactured nanoparticles in natural soils, since most of these factors are closely related in such media. Studies evaluating the simultaneous effects of several soil factors on NPs mobility are clearly needed to elucidate the key soil properties that control NPs transport.

The objective of this study is to determine the influence of soil texture and OM content on the transport of two relevant manufactured nanoparticles, CuO-NPs and TiO_2-NPs in contrasted soils. We conducted water-saturated column experiments with six agricultural soils with contrasted physicochemical properties. For this, we implemented 3 different soil textures: from sandy to clayey soils, and two OM contents for each soil texture. The measured NP breakthrough curves were fitted with the Convection Dispersion Equation (CDE) to identify the dominant processes involved in the transfer of these two NPs in the soils and to quantify the corresponding parameters.

Material and methods

Soils

This study was conducted with soils belonging to three different textural classes: sandy-loam,

85 loam and silty-clay. Soils were collected from the upper 20 cm layer of three different
86 agricultural sites located in the Rhône-Alpes and Burgundy regions of France (see Simonin *et*
87 *al.,* 2015 for further details). At each site, the sampling was performed in two plots with low
88 and high OM contents distant of less than 500 m. Therefore, the experiments were performed
89 with six test soils with three different textures and two different OM contents for each texture.
90 After collection, visible rocks, roots and plant litter of poor reactivity were manually removed.
91 The soils were sieved (2 mm) and homogenized before storage at 4°C. These soils were
92 previously characterized (Simonin *et al.* 2015) and some soil physicochemical properties are
93 presented in Table 1.
94 Soil solutions from the six soils were prepared following the protocol described by Simonin *et*
95 *al.,* (2015) and used as background leaching solutions in the column breakthrough experiments.
96 Briefly, soil solutions were prepared by agitating 10 g of fresh soil dispersed in 50 mL of
97 ultrapure water during 30 minutes at 180 rpm and 20°C in a refrigerated incubator shaker (New
98 Brunswick - Eppendorf, Hamburg, Germany). The solutions were then centrifuged for 20 min
99 at 8000 g, 20°C (Centrifuge 5804R, Eppendorf, Hamburg, Germany) to eliminate particles
100 larger than 20 nm according to the Stokes' law. The supernatants were collected and stored at
101 4°C before characterization (Table 2) and used for NPs suspensions preparation (dispersion by
102 vortexing the suspension 2 min. at maximum speed) and application in column experiments. In
103 these soil solutions, orthophosphate concentrations were determined by Ion chromatography
104 (Metrohm 732/733 separation center).

105 **Nanoparticles**

106 TiO_2-NPs were provided in powder form by Sigma Aldrich (St Louis, USA) with crystal
107 structure of anatase (80%) and rutile (20%) and 99.5% purity. These TiO_2-NPs presented a
108 specific surface area of 35-65 m^2 g^{-1} and a mean particle size of 21 nm as assessed by
109 Transmission Electron Microscopy. CuO-NPs were also purchased from Sigma Aldrich in

110 powder form with a nominal size around 50 nm and a specific surface area of 23 m^2 g^{-1},
111 according to the manufacturer's information. Both NPs were used as bare NPs without any
112 coating and were characterized for intrinsic primary particle size using a ZEISS Ultra 55
113 scanning electron microscopy – field emission gun (SEM-FEG). In average, TiO_2-NPs
114 measured 28.7 ± 7.1 nm and CuO-NPs measured 57.0 ± 18 nm.
115 The apparent hydrodynamic diameter and zeta potential of the NPs were characterized using
116 Dynamic Light Scattering (DLS) with a NanoZS (Malvern) directly in the soil solutions.

117 The measurements were performed in triplicate after dispersion through ultrasonication for 5
118 min in the spiking suspensions of NPs prepared at 50 mg L^{-1} in soil solutions.

119 **Column experiments**

120 The soil solutions were used as background leaching solutions for the duplicated column
121 experiments. Spiking suspensions of NPs at 50 mg L^{-1} were prepared and injected in columns
122 only after ultrasonication for 5 min. This NPs concentration is in the lower range of
123 concentrations found in literature for similar transport studies in natural soils (e.g. Cornelis *et*
124 *al.* 2014). The transport experiments were performed in small glass columns (C10/10, GE
125 Healthcare) of 1 cm in diameter and 10 cm long, homogeneously packed with 8 cm of wet soil
126 as described by Martins and Mermoud (1999), corresponding to approximately 8 g of dry soil.
127 Flow adaptors (AC 10, GE Healthcare) were adjusted on the top of the columns to ensure a
128 constant soil height during experiments. Soil bulk density values are presented in Table 3, along
129 with the values of porosity and volume of pore water. At the beginning of the experiments, soil
130 columns were saturated and leached from bottom to top with 100 mL of freshly prepared soil
131 solution. The effluents were collected using a fraction collector (Gilson 203A) to check for the
132 turbidity of the outflow by measuring the absorbance at 600 nm (Spectrometer Biowave II,
133 Biochrom WPA). The absorbance was very low for all soils (< 0.02), indicating that the amount

134 of soil colloids in the effluents was negligible. Bromide (Br) ion was used as water tracer to
135 assess the hydrodynamic properties of the soils before NPs injection. About two pore volumes
136 of bromide tracer (KBr 1 g L^{-1} also prepared in soil solution) were injected in each soil column
137 and followed by 2 pore volumes injection of bromide-free soil solution. The concentrations of
138 Br^- in the soil column effluents were measured by Ion chromatography (Metrohm 732/733
139 separation center) with a detection limit of 4 µg L^{-1}.

140 The spiking suspensions of NPs (TiO_2 or CuO) prepared at 50 mg L^{-1} (C0) in soil solution were
141 injected in the columns at a flow rate of 0.1 mL min^{-1} during around 4 to 6 pore volumes. After
142 NPs spiking, the columns were continuously leached with soil solution for at least 15 pore
143 volumes. The column effluents were sampled in 15 mL centrifuge tubes every 10 minutes (~1
144 mL collected). Total concentrations of titanium (Ti) or copper (Cu) were measured in the
145 spiking suspensions (C0) and in the effluents (C). The breakthrough curves of NPs are presented
146 in a dimensionless form: C/Co as a function of V/Vo, the dimensionless eluted volume, with V
147 normalized by Vo, the total pore water volume in the saturated column. All column experiments
148 were performed in duplicate.
149 Metal concentration analyses were performed using microwave-assisted (Novawave, SCP
150 Science) strong acid extraction (for Ti: hydrofluoric acid + nitric acid and for Cu: *aqua regia*).
151 Cu and Ti concentrations were determined using inductively coupled plasma optical emission
152 spectrophotometer (ICP-OES; Varian 700-ES, Varian Inc. Scientific Instruments, Palo Alto,
153 USA). With this methodology, Ti and Cu concentrations measured in a certified soil reference
154 material (sandy loam 10, RTC-CRM027, lot HC027, Sigma-Aldrich) were in good agreement
155 with certified values (95−102%). The detection limit was 50 µg L^{-1} for both Cu and Ti
156 measurements. For each soil, breakthrough experiments were performed in control columns by
157 injecting only soil solutions without NPs to determine the background concentration of Ti and
158 Cu in the effluents. This background concentration was then subtracted from the measured

concentrations of Ti and Cu in the effluents. The main characteristics of the soil columns are provided in Table 3.

Determining concentration profiles of Ti and Cu along the soil columns after NPs breakthrough was an important objective of the work. However, the soils used contain naturally relatively high background concentrations of Ti and Cu (measured at 2400-5300 mg kg^{-1} and 10-26 mg kg^{-1}, respectively, Table 1). For Ti, the injected amount of ~ 175 µg by soil column represents about 0.3-0.7% of the natural background Ti concentration present in the column. For Cu, the same injected quantity is close to the soil Cu background concentration. Consequently, as already reported (Nickel et al. (2015) who used concentrations several orders of magnitude higher than in this study (5 g/L), due to solid Ti and Cu contents in these and in other soils, it is not possible to quantify the metals sorbed from the spiking solution, when using environmentally relevant NP concentrations, at least without specific NPs labeling (Vitorge *et al.* 2013), which was indeed not the case in this work.

To evaluate the occurrence of CuO dissolution in spiking suspensions during each column experiment, a dissolution test was performed. The six NPs spiking suspensions (one for each soil) were prepared and sampled (5 mL) after 6 hours corresponding to the maximum duration of the NPs column transport experiments. Dissolved Cu concentration in samples were determined by ICP-OES (Varian 700-ES) after centrifugation for 20 min at 6000 g in a 5 kDa ultrafiltration device (Vivaspin tube, Sartorius). Soil solutions without CuO-NPs were used as controls. The dissolution of TiO_2-NPs in spiking suspensions was not assessed because these NPs are not soluble in water (Chen and Mao 2007; Duester *et al.* 2011).

Transport parameters estimation

The CXTFIT code implemented in the STANMOD software (USDA) (Toride *et al.* 1995) was

183 used to fit the tracer and NPs breakthrough curves. The pore water velocity (v, cm h^{-1}) and
184 dispersion (D, cm^2 s^{-1}) in the NPs transport simulations were determined from the bromide
185 tracer breakthrough curves obtained in the same soil. The analytic solution of the Convection
186 Dispersion Equation (CDE) with a first-order loss term, μ, presented in Eq.1 was fitted to the
187 bromide and NPs breakthrough curves using the Levenberg Maquardt algorithm (e.g. Martins
188 and Mermoud 1999 ; Martins *et al.* 2013; Vitorge *et al.* 2013; Lakshmanan *et al.* 2015).

189 $$R\frac{\partial C}{\partial t} = D\frac{\partial^2 C}{\partial z^2} - v\frac{\partial C}{\partial z} - \mu C \qquad \text{Eq.1}$$

190 where C is the NPs or tracer concentration, R is the retardation factor (dimensionless) of NPs
191 (ratio of NPs and tracer residence times in soil columns), t is time, z is the distance from the
192 inlet, v is the average pore water velocity calculated by dividing the water flow by the column
193 section and the soil volumetric water content, D is the soil dispersion coefficient and μ is the
194 NPs decay coefficient, related to their irreversible retention on solid collectors (soil
195 constituents). For bromide experiments, only v, R and D parameters were calculated. For NPs
196 experiments the parameters v, R, D and μ were calculated for the fitting of the breakthrough
197 curves, using the values determined for the tracer as initial fitting values.

198

199 **Characterization of soil organic matter by infrared spectroscopy**

200 To evaluate the differences in organic matter quality between the 6 soils in relation to soil
201 interactions with CuO-NPs, both soils samples and soils solutions were analyzed by MIR-ATR
202 spectroscopy. Prior to infrared soil spectra acquisition, the six soil samples were prepared as
203 follows: soils were air-dried for 10 days after dry sieving at 2 mm. The fine soil fraction was
204 then finely ground (0.25 mm) using an ultra-centrifugal mill (ZM 200, Retsch) and further dried
205 over-night at 40 °C without altering soil organic matter. MIR measurements were performed

206 using Fourier-transform diamond attenuated total reflectance (MIR-ATR) on ca. 50 mg aliquots
207 with an iS10 spectrometer (Thermo Scientific). MIR-ATR spectra were obtained after
208 correction for interferences by H_2O and CO_2, by averaging 16 scans per sample at a 4 cm^{-1}
209 resolution over the spectral range [4000–400 cm^{-1}]. MIR-ATR measurements of the six soil
210 solutions were performed using Fourier-transform diffuse reflectance on 50µL (1 drop) with
211 the same equipment from Thermo Scientific. Deionized water was used as background solution.
212 The ATR spectrum of water was automatically deduced from the samples spectra for
213 normalization.

214

215 **Statistical analysis**

216 The results of NPs hydrodynamic diameter, zeta potential and dissolution in soil solutions are
217 presented as means (± standard errors) of 3 replicates. The influence of soil texture and OM
218 content on NPs hydrodynamic diameter and zeta potential was investigated with a two-way
219 Anova using the R software.

220

221 Results and discussion

222

223 **Physicochemical properties of nanoparticles in soil solutions**

224 *Apparent size*

225 CuO and TiO_2-NPs were characterized in the six soil solutions used for preparing the spiking
226 suspensions in the transport experiments (Figure 1). The values of hydrodynamic diameter of
227 TiO_2-NPs ranged from 73.9 to 128.1 nm, which is 2.7 to 4.6 times their intrinsic size of 28.7 ±
228 7.1 nm measured by SEM.

229 The content of solid OM in soil appears to only weakly affect the hydrodynamic parameters of
230 NPs (Figure 1A): A marked difference is noted only for the Silty-Clay soil (Figure 1A). The
231 difference relates probably more to the contrasted DOC and Ca content in these two soils (Table
232 2). DOC is known to facilitate colloids dispersion and stabilization (French *et al.* 2009; Badawy
233 *et al.* 2010; Simonin *et al.* 2015; Qiu *et al.* 2020) whereas Ca is known to complex and
234 neutralize, i.e. to precipitate DOC. Coherently, the soil of lowest DOC is that of highest Ca
235 content (the high OM silty-clay soil, Table 2) and the NP's hydrodynamic diameter differs
236 significantly from its sister soil (Low OM silty-clay soil). DOC thus appears to affect the
237 hydrodynamic parameters of NPs more than soil texture.
238 In comparison, the CuO-NPs hydrodynamic diameter values of 53.3 to 84.1 nm are lower than
239 those of TiO_2-NPs. These values measured in the soil solutions were close to the intrinsic value
240 of 57 ± 18 nm measured by SEM. No significant influence of soil texture or OM content on
241 CuO-NPs aggregation was observed (Figure 1B). These results evidence that CuO-NPs are less
242 aggregated than TiO_2-NPs in all soil solutions, except in that of the loam soil with high OM
243 (Figure 1B). The point of zero net proton charge (PZNPC) of Rutile and Anatase is 5.3 and 5.4
244 (Machesky et al., 1994; Kosmulski, 2002), so TiO_2-NPs are negatively charged at circumneutral
245 pH in pure water (Simonin et al., 2015). On the other hand, the PZNPC of native CuO-NPs is
246 equal to 10, they are therefore positively charged in pure water at circumneutral pH. Supposedly
247 the association of the CuO NP's with soil DOM decreases their charge down to negative values,
248 favoring their stabilization. Such a charge inversion effect was observed for CuO NP – humic
249 acid suspensions (Sousa and Teixeira 2013). Possibly, this charge relationship explains the
250 observed higher stability of CuO NPs versus TiO_2-NPs.
251 *Zeta potential*
252 Both TiO_2 and CuO-NPs presented negative zeta potentials in all soil solutions (Figure 1C and
253 1D). The zeta potential of TiO_2-NPs ranged from -23.9 to -15.5 mV whereas that of the CuO-

254 NPs ranged between -20.8 nm and -13.8 mV. For CuO-NPs in contact with Aldrich humic
255 acids, similar negative zeta potentials were observed at similar pH and ionic strength (Sousa
256 and Teixeira, 2013). This comparison suggests that dissolved OM and Aldrich humic acids have
257 similar effects on NPs zeta potential. This result is conceptually in agreement with recent
258 findings, which show that humic acids are constituted as loosely bound molecules of relatively
259 small size, which compare to DOM in terms of composition and acid-base reactivity and
260 consequently charge density (Hruška *et al.* 2003; Sutton and Sposito 2005; Causse *et al.* 2013).
261 The zeta potential of CuO-NPs in soil solutions with high OM content were consistently more
262 negative than in solutions of low OM content, while the observation is reverse for TiO_2-NPs.
263 This surprising behavior is probably related to the high affinity of Cu for OM (Jacobson *et al.*
264 2007; Morel *et al.* 2014; Navel and Martins 2014), which can result in a greater OM coating
265 effect on CuO-NPs compared to TiO_2-NPs and consequently decreased surface charge and zeta
266 potential. Such effects are known to possibly lead to variable NPs surface charge in distinct
267 soils (Simonin et al. 2015).
268
269 **Hydrodynamic properties of the soils**
270 The hydrodynamic properties of the six soils were determined by fitting the breakthrough
271 curves of the water tracer, the bromide ion, with the CXTFIT code (Figure 2A). The
272 corresponding transport parameters are presented in Table 4 with those adjusted for the CuO-
273 NPs and TiO_2-NPs. All bromide breakthrough curves presented mass recoveries close to 100%,
274 as expected with an inert water tracer. Retardation factors (R) of bromide were all close to 1,
275 except that calculated in the silty-clay- high OM soil. In this soil, R was 0.81, which indicates
276 that some of the pore water was not traced by the water tracer, probably in relation with the
277 high clay content of this soil and/or ionic exclusion or poorly accessible immobile water
278 (Monrozier et al. 1993). Dispersion values (D) fitted to the breakthrough curves are quite low

279 (below 10^{-7} cm^2 s^{-1}) and almost similar for all soils. These parameter values were used as initial
280 D values in CXTFIT to fit the breakthrough curves of the NPs in the corresponding soils.
281
282 **Transport of TiO_2-NPs in soil columns**
283 The mobility of TiO_2-NPs was found to be very low in all soils, with mass recoveries ranging
284 between 1.9 and 5.5% (Table 4). These NPs breakthrough curves measured in the six soils were
285 very noisy, indicating that the measured Ti concentrations were in the range of Ti background
286 concentration in the leachates (Figure 2B). Consequently, transport modelling was not possible
287 for the TiO_2-NPs breakthrough curves. In all soils the irreversible retention of TiO_2-NPs was
288 higher than CuO-NPs. This strong retention probably relates to the observed higher
289 homoaggregation of TiO_2-NPs in soil solutions, which increased the apparent NPs' size by a
290 factor of 2.5 to 4.5 (Figure 1) in agreement with Vitorge *et al.* (2013). No clear influence of the
291 soil OM content on TiO_2-NPs mobility could be evidenced in the six soils, because of their very
292 low mobility. These results contrast with previous studies on the mobility of TiO_2-NPs
293 conducted in columns of glass beads or sand material, which usually present these NPs as
294 mobile especially at alkaline pH (Ben-Moshe, Dror and Berkowitz 2010; Solovitch *et al.* 2010;
295 Chowdhury, Cwiertny and Walker 2012; Rastghalam *et al.* 2019). However, our results are
296 consistent with previous works conducted in natural soils by Wang *et al.* (2014) or Nickel *et al.*
297 (2015), although these experiments were performed with positively charged TiO_2-NPs. A study
298 performed in natural soils is in significant disagreement with strong retention of TiO_2 NPs (Fang
299 *et al.* 2009). They used negatively charged TiO_2-NPs as in our study but observed a significant
300 transport of these NPs, especially in soils with low clay, high DOM content and low ionic
301 strength. Their DOC values are all much higher than those of our study (factor ~ 7), which
302 could indicate a dominant effect of this factor on NPs mobility, especially considering their
303 rather similar or even decreased Ca^{++} values. In this study, NPs are transferred as a tracer

304 especially at high DOM content. Fang et al., (2016) observed a similar behavior of TiO_2 NPs
305 in the presence of fulvic acids. Since in our experiments, the retention of TiO_2-NPs was very
306 high in the six soils studied, it was not possible to observe any influence of the soil texture (soil
307 clay content) or of the ionic strength of soil solution. In our six soils, TiO_2-NPs were not
308 transported deeper than 8 cm. This result may relate to the relatively low DOM content of the
309 soils, low NPs input concentration and/or other parameters such as soil aggregation column size
310 and setup. Studying the fate of TiO_2-NPs in soil is very challenging as Ti is abundant in soils
311 and presents a very heterogeneous distribution. The findings obtained with laboratory saturated
312 soil columns give a first assessment of the risk of NPs migration to deeper soil layers or
313 groundwater, which appears very low. However, further work is clearly needed to assess the
314 mobility potential of TiO_2-NPs at environmentally relevant concentrations, in undisturbed soils
315 or under unsaturated conditions and simulating repeated exposures in order to be closer to
316 expected field conditions (Duester *et al.* 2011; Cornelis *et al.* 2014; Conway and Keller 2016;
317 Simonin *et al.* 2016).
318
319 **Chemical stability and transport of CuO-NPs in soil columns**
320 In order to calculate accurate mass balances for the column NPs-displacement experiments, the
321 ability of CuO-NPs to dissolve in the six soils solutions was first assessed in the spiking
322 suspensions through a 6-hour kinetic study. CuO-NPs dissolution was found to be negligible in
323 all soil solutions, ranging from 0.22 and 0.49 % of the NPs applied mass (50 mg/L), after 6
324 hours of contact, which represents the maximum residence time of the NPs in the columns
325 during transport experiments (Table 2). The measured aqueous Cu concentrations ranged from
326 0.112 to 0.243 mg L^{-1} that situate all below the PHREEQC-calculated Cu solubility limits
327 toward Tenorite (Parkhurst and Appelo 2013). This evidences a slow dissolution kinetic of the
328 NPs. Consequently, Cu concentrations measured in the effluents can be attributed to CuO-NPs

329 and not to dissolved Cu species.

330 All CuO-NPs breakthrough curves were fitted with the Convection Dispersion Equation, using
331 the hydrodynamic parameters determined with the water tracer. The observed and CDE-Fitted
332 breakthrough curves of CuO-NPs are presented in Figure 2A together with those of the water
333 tracer (Br). The corresponding parameters are presented in Table 4. The CuO-NPs breakthrough
334 curves (Figure 2A) show that these NPs are only partially mobile in the six soils, as important
335 amounts of NPs were irreversibly retained in all soils, with NPs mass recoveries ranging from
336 5.2 to 14% (Table 4). Unlike TiO_2-NPs, the partial mobility of CuO-NPs provided breakthrough
337 curves that can be used to assess the influence of the studied factors on the transport of CuO-
338 NPs. In all soils, the eluted CuO-NPs presented a fast transport through soil columns with no
339 or low retardation as compared to the bromide tracer (Table 4). No clear effect of soil texture
340 could be observed with the tested soils and, in particular, CuO-NPs were not specifically more
341 mobile in the sandy-loam soils than in the loam or silty-clay soils as commonly observed for
342 other types of pollutants (pesticides, PAH, heavy metals...) and as expected from previous work
343 (Fang *et al.* 2009). In the sandy-loam soils, CuO-NPs were transported slightly faster than the
344 tracer (R = 0.98 and 0.91) indicating that in this type of soil, the NPs do not "see" all the water
345 present in the soil presumably due to size exclusion processes or exclusion from immobile water
346 zone during their transport (Table 4). In the loam and silty-clay soils, the CuO-NPs were
347 transported slightly slower than water and presented a retardation factor slightly higher than 1,
348 especially in the low OM soils. As for the tracer, the retardation factor measured in the high
349 OM soils appeared always lower than in the low OM soils, indicating a clear relation between
350 NPs mobility and soil OM content. This is possibly related to an increased soil structuration
351 induced by the higher OM content in soil compared to the low OM soils (Jastrow 1996; Álvaro-
352 Fuentes *et al.* 2009). Such soil structuration improvement is indeed known to increase soil
353 permeability through the formation of slightly bigger pores, which can facilitate the transfer of

354 colloids or bacteria (Martins *et al.* 2013; Vitorge *et al.* 2013; Bagheri *et al.* 2019). Under our
355 conditions, the different apparent size and zeta potential values of CuO-NPs measured in the
356 different soil solutions do not seem to significantly affect NPs mobility whatever the soil. In
357 the two loam soils of low and high OM contents, the CuO-NPs breakthrough curves were indeed
358 very similar (Figure 2A), although their zeta potential values were the most contrasted (Figure
359 1), indicating that electrostatic interactions are probably not the dominant NPs retention process
360 in the tested soils.
361 While in loam soils the NPs breakthrough curves were very similar in both low and high OM
362 content conditions, in the sandy-loam and silty-clay soils, the breakthrough curves varied
363 oppositely between the high and low OM condition (Figure 2). Interestingly, the mobility
364 (recovery rate) of CuO-NPs increased by 62% in the high OM - sandy-loam soil compared to
365 the low OM one, while in the silty-clay soil, CuO-NPs mobility decreased by 44% in the high
366 OM soil compared to the low OM soil (Table 4, Figure 2A).
367 In the sandy-loam (high OM) and the silty-clay (low OM) soils, where CuO-NPs transport was
368 enhanced, the concentration of dissolved organic carbon (DOC) in soil solutions was
369 significantly higher than in the four other soils (Table 2). DOC concentration in soil solution
370 appears thus as an important factor in NPs mobility, as has already been demonstrated in less
371 complex porous media (e.g. Ben-Moshe *et al.* 2010; Rastghalam *et al.* 2019). Other factors are
372 probably also involved in the higher mobility of CuO-NPs in these two soils (e.g., low Ca and
373 Mg concentrations in soil solutions). Although several studies have evaluated the mobility of
374 CuO-NPs in columns of glass beads or sand material (Ben-Moshe, Dror and Berkowitz 2010;
375 Wu *et al.* 2020), this study is one of the first studies on the transport of CuO-NPs in a series of
376 6 agricultural soils. We have shown here that CuO-NPs are partly mobile in all the contrasted
377 soils studied, although the majority (86 to 94.2%) of these NPs are retained in the 8 cm top
378 layer of these soils.

379

380 **Spectral characteristics of soils and soils solutions**

381 To further assess the observed differences in the effects of solid and dissolved OM levels on
382 CuO-NPs mobility, a comparison of the MIR-ATR spectra of the six soils and of the six soil
383 solutions is presented in Figure 3. For the solid phase, all the MIR-ATR spectra are mainly
384 dominated by the strong absorption of soil minerals, which are very similar for the six soils.
385 Only slight insignificant spectral differences can be observed between the spectra obtained with
386 low and high OM soils (Figure 3A), which do not explain the observed differences in the
387 mobility of CuO-NPs. According to Stenberg *et al.* (2010) and Erktan *et al.* (2016), the most
388 frequent peaks in the MIR-ATR spectra of soils correspond to phyllosilicates (3622, 1635, 988,
389 and 795 cm^{-1}) and/or iron (oxy)hydroxydes (3622 and 795 cm^{-1}) and tannins (1612, 1450, and
390 669 cm^{-1}), with carboxylate (1592 and 1417 cm^{-1}, respectively), alkyl (CH_2 and CH_3 bending
391 vibrations at 1455 and 1380 cm^{-1}, respectively) and aromatic moieties (phenol O–H bend at
392 1370 cm^{-1}). The relatively low organic carbon content (a few %) of soils (Table 1) may explain
393 the dominant absorption of soil minerals in mid-infrared.

394 For soils solutions (Figure 3B), although the MIR spectra appear very similar, slight differences
395 can be observed in the 1200-980 cm^{-1} IR range of interest (black rectangles). Although
396 incomplete correction of the background atmosphere (CO2) could have occurred, this is
397 particularly visible in the wavelength ranges relating to dissolved inorganic phosphorus
398 species(e.g. Tammer 2004; Elzinga and Sparks 2007; Klein *et al.* 2019). In this range, slightly
399 higher or lower absorptions, corresponding to different Phosphate species were observed for
400 the Sandy-Loam (high OM) and Silty-Clay (low OM) soil solutions, which are precisely the
401 soils in which the mobility of CuO-NPs was highest (Figure 2). On the contrary, MIR
402 absorption was lowest or highest in this range for the Sandy-Loam (low OM) and Silty-Clay
403 (high OM) in which CuO-NPs mobility was lowest. In the 980 to 1200cm^{-1} range, IR absorption

404 was very similar for the solutions of the two loam soils, in which CuO-NPs transport was very
405 similar. For the sandy-Loam (high OM) and silty-Clay (low OM) soils, chemical analysis of P
406 in soil solutions (Table 2) is in agreement with these IR trends and confirms the presence of
407 higher concentrations of dissolved phosphate in the soils in which CuO-NPs are the more
408 mobile. These results clearly suggest the existence of interactions between CuO-NPs and
409 dissolved phosphorous (P) species in the soils that could explain the better stability of NPs in
410 solution and therefore their slightly higher mobility in soils.
411
412 **Phosphate effect on NPs transport**
413 Phosphate is known to strongly sorb on metal oxides (e.g. Fe, Cu and Al oxides) even in acidic
414 natural environments (Mahdavi and Akhzari 2016; Claudio *et al.* 2017; Klein *et al.* 2019).
415 These properties have been used for various purposes, such as in agronomy to enhance
416 phosphorus phytoavailability in soil (Zahra *et al.* 2015) or in wastewater treatment to eliminate
417 phosphorus species (Acelas *et al.* 2015).
418 Our data suggest that phosphate species increase the mobility of CuO-NPs in the soils studied.
419 Several studies performed in quartz sand columns suggested a similar positive influence of
420 phosphorus species on several types of NPs and especially of TiO_2-NPs (Hou *et al.* 2017;
421 Rastghalam *et al.* 2018; Xu *et al.* 2020). Xu et al. (2018) studying a TiO_2 NP's - phosphate -
422 bacteria ternary system showed that phosphate species generally facilitates the transport of TiO_2
423 NPs linked on bacteria except in the presence of Fe oxide coatings or of low phosphate
424 concentrations.
425 The main effect of phosphate appears to be the decrease of NPs surface charge induced by
426 phosphate sorption. The stronger negative zeta potential of NPs probably results in enhanced
427 repulsion of similarly charged soil constituents and, consequently, in the better stability and
428 facilitated transfer of NPs in soil. In addition, the high complexing capacity of P may enable

429 the formation of ternary complexes and, consequently, bridges between positively charged
430 moieties, which are relevant for soils (Sheng *et al.* 2019; Mendez and Hiemstra 2020). Zhara
431 et al. (2015) suggested that positively charged TiO_2-NPs, are destabilized by inter-particular
432 phosphate bridges. Concerning Xu et al (2018), supposedly phosphate species bridge NPs to
433 positively charged Fe oxide surfaces, as long as sorbed phosphate does not inverse the Fe oxide
434 surface charge.
435 Globally, the effect of phosphate on NPs appears to be diverse. A facilitation of transport and
436 dispersion effect linked to the negative charge of the sorbed phosphate species is potentially
437 associated with an opposite immobilizing and aggregation effect linked to phosphate ternary
438 bridging. Based on our observations, this study suggests that the apparent charge effect appears
439 to be the dominant process under our conditions.
440
441 In conclusion, this study demonstrated a low or very low mobility of CuO and TiO_2-NPs in
442 agricultural soils, respectively. When differences in NP mobility were observed between soils,
443 they seemed to be mainly due to dissolved OC and phosphate concentrations in soil solution.
444 Globally, the low mobility of NPs observed in an 8 cm soil layer in this study suggests that
445 these two NPs present a low risk of direct groundwater contamination in a wide range of surface
446 soils, although mobilization mechanism effects, probably involving P species, could increase
447 this mobility and thus the associated risk for water supply. This low mobility also raises
448 concerns about the long-term impacts of NPs on plants and soil biodiversity in agroecosystems
449 that would require to be investigated under realistic field conditions.
450

451 ## Acknowledgments

452 Marie Simonin was supported by a Ph.D grant from Rhône-Alpes Region – ARC

Environnement. This work was funded by a grant from the French National Program Microbien EC2CO-CNRS. The authors thank the lab assistance of Erwann Vince and Sophie Sebastianutti (MOME and AirOsol platforms at IGE) and also of Alix Dumay for modelling assistance. Special thanks are due to Lauric Cécillon and Alejandro Fernandez-Martinez for Infrared spectra measurements and help for interpretation. IGE is part of the Labex OSUG@2020 (ANR10 LABX56). We thank the Equipex NanoID (ANR-10-EQPX-39) for the access to the NanoZS (ISTerre).

Conflict of interest

The authors declare no conflict of interest.

References

Acelas NY, Martin BD, López D *et al.* Selective removal of phosphate from wastewater using hydrated metal oxides dispersed within anionic exchange media. *Chemosphere* 2015;**119**:1353–60.

Álvaro-Fuentes J, Cantero-Martínez C, López MV *et al.* Soil Aggregation and Soil Organic Carbon Stabilization: Effects of Management in Semiarid Mediterranean Agroecosystems. *Soil Science Society of America Journal* 2009;**73**:1519–29.

Badawy AME, Luxton TP, Silva RG *et al.* Impact of Environmental Conditions (pH, Ionic Strength, and Electrolyte Type) on the Surface Charge and Aggregation of Silver Nanoparticles Suspensions. *Environ Sci Technol* 2010;**44**:1260–6.

Bagheri H, Zare Abyaneh H, Izady A *et al.* Modeling the transport of nitrate and natural multi-sized colloids in natural soil and soil amended with vermicompost. *Geoderma* 2019;**354**:113889.

Ben-Moshe T, Dror I, Berkowitz B. Transport of metal oxide nanoparticles in saturated porous media. *Chemosphere* 2010;**81**:387–93.

Braun A, Klumpp E, Azzam R *et al.* Transport and deposition of stabilized engineered silver nanoparticles in water saturated loamy sand and silty loam. *Science of The Total Environment* 2015;**535**:102–12.

Causse B, Spadini L, Martins JMF *et al.* Xanthan exopolysaccharide: Acid–base reactivity related to structure and conformation. A model for understanding the reactivity of degraded and colloidal soil organic matter. *Chemical Geology* 2013;**359**:150–8.

Chekli L, Brunetti G, Marzouk ER *et al.* Evaluating the mobility of polymer-stabilised zero-valent iron nanoparticles and their potential to co-transport contaminants in intact soil cores. *Environmental Pollution* 2016;**216**:636–45.

Chen X, Mao SS. Titanium Dioxide Nanomaterials: Synthesis, Properties, Modifications, and Applications. *Chem Rev* 2007;**107**:2891–959.

Chowdhury I, Cwiertny DM, Walker SL. Combined Factors Influencing the Aggregation and Deposition of nano-TiO2 in the Presence of Humic Acid and Bacteria. *Environ Sci Technol* 2012;**46**:6968–76.

Claudio C, Iorio E di, Liu Q *et al.* Iron Oxide Nanoparticles in Soils: Environmental and Agronomic Importance. *Journal of Nanoscience and Nanotechnology* 2017;**17**:4449–60.

Conway JR, Keller AA. Gravity-driven transport of three engineered nanomaterials in unsaturated soils and their effects on soil pH and nutrient release. *Water Research* 2016;**98**:250–60.

Cornelis G, Hund-Rinke K, Kuhlbusch T *et al.* Fate and Bioavailability of Engineered Nanoparticles in Soils: A Review. *Critical Reviews in Environmental Science and Technology* 2014;**44**:2720–64.

Cornelis G, Pang L, Doolette C *et al.* Transport of silver nanoparticles in saturated columns of natural soils. *Science of The Total Environment* 2013;**463–464**:120–30.

Duester L, Prasse C, Vogel JV *et al.* Translocation of Sb and Ti in an undisturbed floodplain soil after application of Sb2O3 and TiO2 nanoparticles to the surface. *J Environ Monit* 2011;**13**:1204–11.

Erktan A, Legout C, De Danieli S *et al.* Comparison of infrared spectroscopy and laser granulometry as alternative methods to estimate soil aggregate stability in Mediterranean badlands. *Geoderma* 2016;**271**:225–33.

Fang J, Shan X, Wen B *et al.* Stability of titania nanoparticles in soil suspensions and transport in saturated homogeneous soil columns. *Environmental Pollution* 2009;**157**:1101–9.

Fang J, Shan X, Wen B *et al.* Transport of copper as affected by titania nanoparticles in soil columns. *Environmental Pollution* 2011;**159**:1248–56.

Fang J, Zhang K, Sun P *et al.* Co-transport of Pb2 + and TiO2 nanoparticles in repacked homogeneous soil columns under saturation condition: Effect of ionic strength and fulvic acid. *Science of The Total Environment* 2016;**571**:471–8.

French RA, Jacobson AR, Kim B *et al.* Influence of Ionic Strength, pH, and Cation Valence on Aggregation Kinetics of Titanium Dioxide Nanoparticles. *Environ Sci Technol* 2009;**43**:1354–9.

Hou J, Zhang M, Wang P *et al.* Transport, retention, and long-term release behavior of polymer-coated silver nanoparticles in saturated quartz sand: The impact of natural organic matters and electrolyte. *Environmental Pollution* 2017;**229**:49–59.

Hruška J, Köhler S, Laudon H *et al.* Is a universal model of organic acidity possible: Comparison of the acid/base properties of dissolved organic carbon in the boreal and temperate zones. *Environmental science & technology* 2003;**37**:1726–30.

Jacobson AR, Dousset S, Andreux F *et al.* Electron Microprobe and Synchrotron X-ray Fluorescence

Mapping of the Heterogeneous Distribution of Copper in High-Copper Vineyard Soils. *Environ Sci Technol* 2007;**41**:6343–9.

Jastrow JD. Soil aggregate formation and the accrual of particulate and mineral-associated organic matter. *Soil Biology and Biochemistry* 1996;**28**:665–76.

Keller AA, McFerran S, Lazareva A *et al.* Global life cycle releases of engineered nanomaterials. *J Nanopart Res* 2013;**15**:1–17.

Klein AR, Bone SE, Bakker E *et al.* Abiotic phosphorus recycling from adsorbed ribonucleotides on a ferrihydrite-type mineral: Probing solution and surface species. *Journal of Colloid and Interface Science* 2019;**547**:171–82.

Lakshmanan S, Holmes WM, Sloan WT *et al.* Nanoparticle transport in saturated porous medium using magnetic resonance imaging. *Chemical Engineering Journal* 2015;**266**:156–62.

Ley TW (Washington SU), Stevens RG, Topielec RR *et al.* Soil water monitoring and measurement. *PNW (USA)* 1994.

Mahdavi S, Akhzari D. The removal of phosphate from aqueous solutions using two nano-structures: copper oxide and carbon tubes. *Clean Techn Environ Policy* 2016;**18**:817–27.

Martins JM, Mermoud A. Sorption and degradation of four nitroaromatic herbicides in mono and multi-solute saturated/unsaturated soil batch systems. *Journal of Contaminant Hydrology* 1998;**33**:187–210.

Martins JMF, Majdalani S, Vitorge E *et al.* Role of macropore flow in the transport of Escherichia coli cells in undisturbed cores of a brown leached soil. *Environ Sci: Processes Impacts* 2013;**15**:347–56.

Mendez JC, Hiemstra T. Ternary Complex Formation of Phosphate with Ca and Mg Ions Binding to Ferrihydrite: Experiments and Mechanisms. *ACS Earth Space Chem* 2020;**4**:545–57.

Morel M-C, Spadini L, Brimo K *et al.* Speciation study in the sulfamethoxazole–copper–pH–soil system: Implications for retention prediction. *Science of The Total Environment* 2014;**481**:266–73.

Navel A, Martins JMF. Effect of long term organic amendments and vegetation of vineyard soils on the microscale distribution and biogeochemistry of copper. *Science of The Total Environment* 2014;**466–467**:681–9.

Nickel C, Gabsch S, Hellack B *et al.* Mobility of coated and uncoated TiO 2 nanomaterials in soil columns–Applicability of the tests methods of OECD TG 312 and 106 for nanomaterials. *Journal of environmental management* 2015;**157**:230–7.

Nowack B, Ranville JF, Diamond S *et al.* Potential scenarios for nanomaterial release and subsequent alteration in the environment. *Environmental Toxicology and Chemistry* 2012;**31**:50–9.

Pan B, Xing B. Applications and implications of manufactured nanoparticles in soils: a review. *European Journal of Soil Science* 2012;**63**:437–56.

Parkhurst DL, Appelo CAJ. *Description of Input and Examples for PHREEQC Version 3: A Computer Program for Speciation, Batch-Reaction, One-Dimensional Transport, and Inverse Geochemical Calculations*. US Geological Survey, 2013.

Qiu Y, Mu Z, Wang N *et al.* The aggregation and sedimentation of two different sized copper oxide nanoparticles in soil solutions: Dependence on pH and dissolved organic matter. *Science of The Total Environment* 2020;**731**:139215.

Rastghalam ZS, Cheng T, Freake B. Fine particle attachment to quartz sand in the presence of multiple interacting dissolved components. *Science of The Total Environment* 2018;**645**:499–508.

Rastghalam ZS, Yan C, Shang J *et al.* Nanoscale titanium dioxide (nTiO2) aggregation and transport in the co-presence of dissolved phosphate, illite colloid, and Fe oxyhydroxide coating. *Colloids and Surfaces A: Physicochemical and Engineering Aspects* 2019;**578**:123560.

Ren G, Hu D, Cheng EWC *et al.* Characterisation of copper oxide nanoparticles for antimicrobial applications. *International Journal of Antimicrobial Agents* 2009;**33**:587–90.

Sheng X, Qin C, Yang B *et al.* Metal cation saturation on montmorillonites facilitates the adsorption of DNA via cation bridging. *Chemosphere* 2019;**235**:670–8.

Simonin M, Guyonnet JP, Martins JMF *et al.* Influence of soil properties on the toxicity of TiO2 nanoparticles on carbon mineralization and bacterial abundance. *Journal of Hazardous Materials* 2015;**283**:529–35.

Simonin M, Martins JMF, Uzu G *et al.* Combined Study of Titanium Dioxide Nanoparticle Transport and Toxicity on Microbial Nitrifying Communities under Single and Repeated Exposures in Soil Columns. *Environ Sci Technol* 2016, DOI: 10.1021/acs.est.6b02415.

Solovitch N, Labille J, Rose J *et al.* Concurrent Aggregation and Deposition of TiO2 Nanoparticles in a Sandy Porous Media. *Environ Sci Technol* 2010;**44**:4897–902.

Sousa VS, Teixeira MR. Aggregation kinetics and surface charge of CuO nanoparticles: the influence of pH, ionic strength and humic acids. *Environ Chem* 2013;**10**:313–22.

Spadini L, Navel A, Martins JMF *et al.* Soil aggregates: a scale to investigate the densities of metal and proton reactive sites of organic matter and clay phases in soil. *European Journal of Soil Science* 2018;**69**:953–61.

Stenberg B, Viscarra Rossel RA, Mouazen AM *et al.* Chapter Five - Visible and Near Infrared Spectroscopy in Soil Science. In: Sparks DL (ed.). *Advances in Agronomy*. Vol 107. Academic Press, 2010, 163–215.

Sutton R, Sposito G. Molecular structure in soil humic substances: the new view. *Environmental science & technology* 2005;**39**:9009–15.

Tammer M. *G. Sokrates: Infrared and Raman Characteristic Group Frequencies: Tables and Charts*. Springer, 2004.

Thio BJR, Zhou D, Keller AA. Influence of natural organic matter on the aggregation and deposition of titanium dioxide nanoparticles. *Journal of Hazardous Materials* 2011;**189**:556–63.

Toride N, Leij FJ, Van Genuchten MT. The CXTFIT code for estimating transport parameters from laboratory and field tracer experiments. 1995.

Vitorge E, Szenknect S, Martins JMF *et al.* Size- and concentration-dependent deposition of

fluorescent silica colloids in saturated sand columns: transport experiments and modeling. *Environ Sci: Processes Impacts* 2013;**15**:1590–600.

Vitorge E, Szenknect S, Martins JMF *et al.* Comparison of three labeled silica nanoparticles used as tracers in transport experiments in porous media. Part I: Syntheses and characterizations. *Environmental Pollution* 2014;**184**:605–12.

Wang D, Su C, Zhang W *et al.* Laboratory assessment of the mobility of water-dispersed engineered nanoparticles in a red soil (Ultisol). *Journal of Hydrology* 2014;**519, Part B**:1677–87.

Wang Y, Gao B, Morales VL *et al.* Transport of titanium dioxide nanoparticles in saturated porous media under various solution chemistry conditions. *J Nanopart Res* 2012;**14**:1–9.

Wu H, Fang H, Xu C *et al.* Transport and retention of copper oxide nanoparticles under unfavorable deposition conditions caused by repulsive van der Waals force in saturated porous media. *Environmental Pollution* 2020;**256**:113400.

Xu N, Li Z, Huangfu X *et al.* Facilitated transport of nTiO2-kaolin aggregates by bacteria and phosphate in water-saturated quartz sand. *Science of The Total Environment* 2020;**713**:136589.

Zahra Z, Arshad M, Ali MA *et al.* Phosphorus Phytoavailability upon Nanoparticle Application. In: Hayat S, Pichtel J, Faizan M, et al. (eds.). *Sustainable Agriculture Reviews 41: Nanotechnology for Plant Growth and Development*. Cham: Springer International Publishing, 2020, 41–61.

Zahra Z, Arshad M, Rafique R *et al.* Metallic Nanoparticle (TiO2 and Fe3O4) Application Modifies Rhizosphere Phosphorus Availability and Uptake by Lactuca sativa. *J Agric Food Chem* 2015;**63**:6876–82.

Zhou D, Abdel-Fattah AI, Keller AA. Clay Particles Destabilize Engineered Nanoparticles in Aqueous Environments. *Environ Sci Technol* 2012;**46**:7520–6.

Zhu J, Li D, Chen H *et al.* Highly dispersed CuO nanoparticles prepared by a novel quick-precipitation method. *Materials Letters* 2004;**58**:3324–7.

620 **TABLES**

621

622 Table 1: Main characteristics of the six studied soils

	% sand	% loam	% clay	% OM	WHC (%)	pH	Ionic strength (mM)	CEC ($cmol^+ kg^{-1}$)	Cu ($mg kg^{-1}$)	Ti ($g kg^{-1}$)
Sandy-loam - Low OM	68.4	14.7	16.9	2.09	20	7.0	0.98	11.5	20.1	2.4
Sandy-loam - High OM	65.6	16.1	18.3	4.46	20	6.9	1.59	15.4	21.9	2.4
Loam - Low OM	37.5	42.7	19.8	2.23	30	6.4	0.60	8.79	13.2	2.7
Loam - High OM	40.3	40.8	18.9	6.77	30	6.3	1.31	15.3	10.4	2.4
Silty-clay - Low OM	8.2	49.8	42.0	4.72	47	6.9	0.51	17.4	23.2	5.3
Silty-clay - High OM	10.1	50.8	39.1	7.87	51	7.7	1.37	20.1	26.2	4.5

623

624

625

626 Table 2: Characteristics of the soil solutions used for the transport experiments (all concentrations are expressed in mg L^{-1}) and results of Cu

627 dissolution test in soil solutions conducted for 6 hours at 50 mg/L CuO-NPs.

	pH	Ionic strength (mM)	DOC	Ca	K	Mg	Na	Al	Fe	Mn	PO_4	Solubility PO_{4_Th}	% of dissolved Cu after 6h	PhreeqC Calc. Cu_{Th} Solubility
Sandy-loam - Low OM	6.7	1.0	11.6	21.7	5.25	2.43	8.89	4.70	1.45	0.02	2.72	1.18	0.27 %	0.68
Sandy-loam - High OM	6.4	2.0	18.6	12.2	6.84	1.11	12.06	7.62	1.69	0.02	3.67	7.47	0.49 %	1.19
Loam - Low OM	6.2	1.2	8.2	28.8	3.84	3.23	13.18	11.35	1.90	0.09	1.19	6.48	0.37 %	3.46
Loam - High OM	5.4	2.4	10.5	38.2	15.57	2.59	21.78	6.66	2.79	0.04	3.85	442.18	0.28 %	64.01
Silty-clay - Low OM	6.3	1.5	25.2	33.5	3.69	1.40	11.41	4.35	1.79	0.01	0.74	3.73	0.24 %	2.74
Silty-clay - High OM	7.1	1.6	8.9	80.8	4.15	4.28	5.48	2.66	3.53	0.04	0.00	0.03	0.22 %	0.4

628 **PO_{4_Th} : Calculated total orthophosphate solubility toward Apatite ; Cu_{Th} : Calculated Cu(II) solubility toward Tenorite without OM.**

Table 3: Main characteristics of the soil columns

	Pore volume (mL)	Bulk density (g cm^{-3})	Effective Porosity	Darcy velocity (cm h^{-1})	Average soil collector diameter* (µm)
Sandy-loam - Low OM	2.90	1.27	0.51	14.9	122.9
Sandy-loam - High OM	3.32	1.08	0.59	13.0	118.3
Loam - Low OM	3.85	0.83	0.68	11.3	74.5
Loam - High OM	3.80	0.86	0.67	11.4	78.9
Silty-clay - Low OM	3.47	1.01	0.61	12.5	24.9
Silty-clay - High OM	3.62	0.94	0.64	12.0	28.4

* Calculations based on Ley *et al.* (1994)

Table 4: Transport parameters for bromide, CuO-NPs and TiO_2–NPs experiments.

		Bromide			CuO-NPs				TiO_2-NPs
		MR (%)	D (cm^2/s)	R (-)	MR (%)	D (cm^2/s)	R (-)	μ (h^{-1})	MR (%)
Sandy-loam	Low OM	97.4	1.0E-07	1.03	5.2	1.35E-05	0.98	7.27	2.1
	High OM	98.8	7.1E-08	0.97	14.0	2.52E-07	0.91	1.97	5.5
Loam	Low OM	97.3	1.0E-07	0.99	11.4	1.10E-08	1.06	2.29	2.3
	High OM	95.1	5.9E-08	0.96	9.7	8.30E-08	0.99	2.37	3.4
Silty-clay	Low OM	96.4	1.2E-07	0.90	12.1	1.04E-05	0.92	2.37	1.9
	High OM	94.8	5.5E-08	0.81	6.8	9.47E-07	0.88	3.28	2.2

MR: Mass Recovery (%), D: Dispersion value, R: Retardation factor

FIGURES

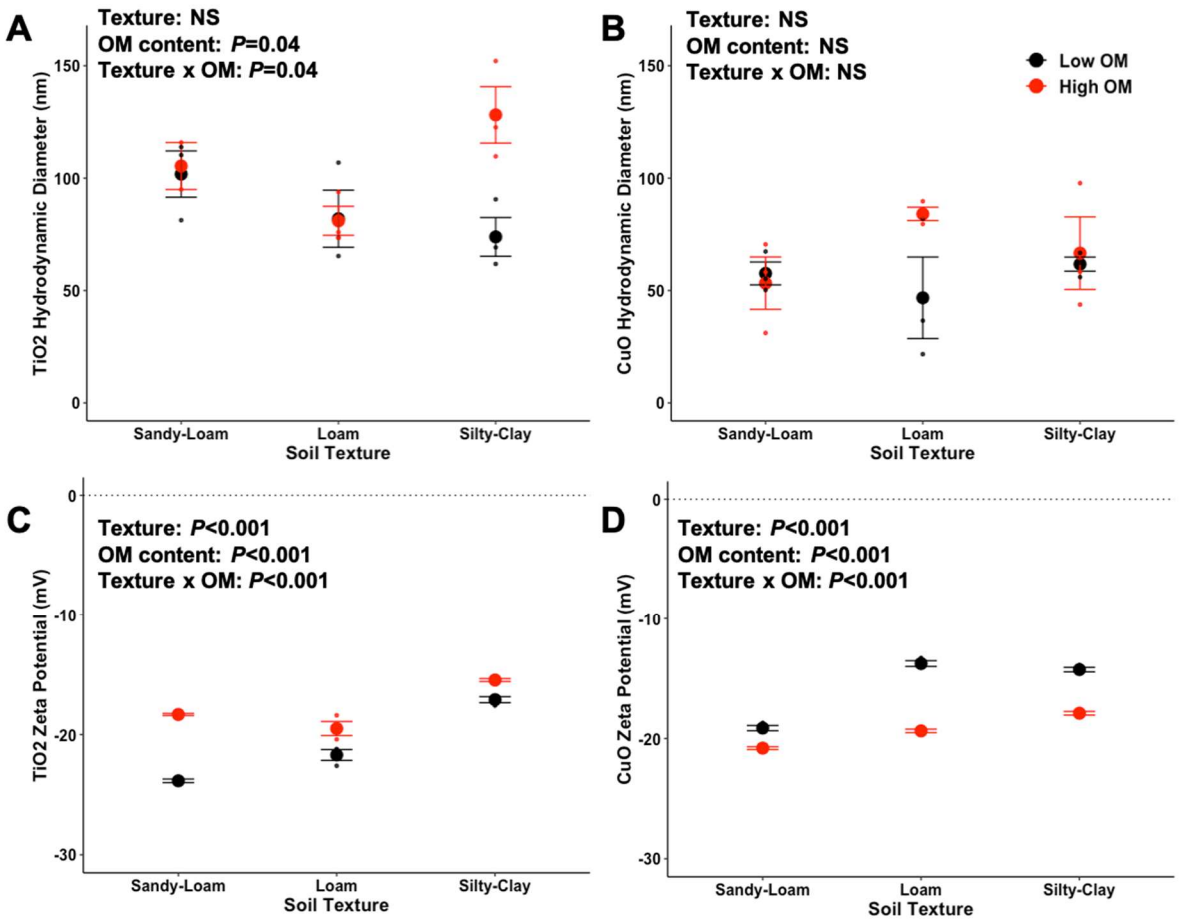

Figure 1: TiO_2 and CuO-NPs hydrodynamic diameter (A and B, respectively) and zeta potential (C and D, respectively) measured in background soil solutions prepared at 50 mg NPs L^{-1} before column transport experiments. The *P*-values associated to the effect of soil texture, OM content and the interaction of texture and OM on the size (i.e. hydrodynamic diameter) and zeta potential of TiO_2 and CuO-NPs are indicated on the top-left corner of each panel (NS: Non-Significant).

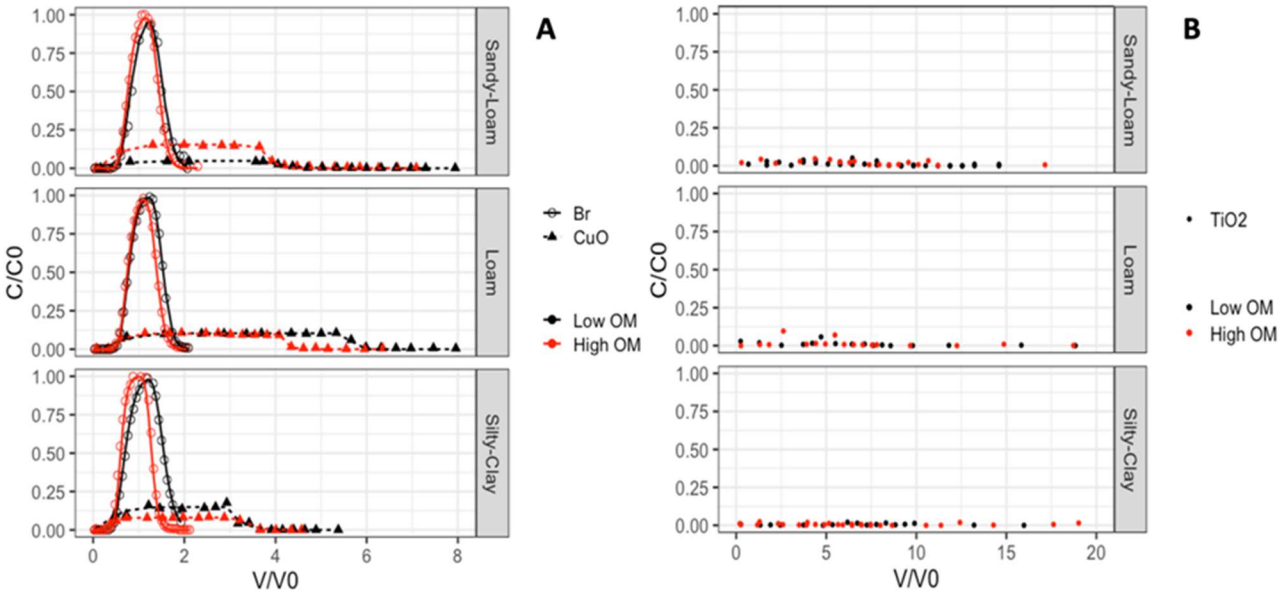

Figure 2: A) Breakthrough curves of the Bromide water tracer and CuO-NPs in columns of the Sandy-Loam, Loam and Silty Clay soils. B) Breakthrough curves of the TiO_2-NPs in the six soils. TiO_2 breakthrough curves could not be fitted due to the low recovery of NPs in the effluents. Symbols represent the element injected in the column (Br, CuO or TiO_2), and solid (Br) and dashed lines (CuO) were calculated with the CXTFIT code by fitting with STANMOD.

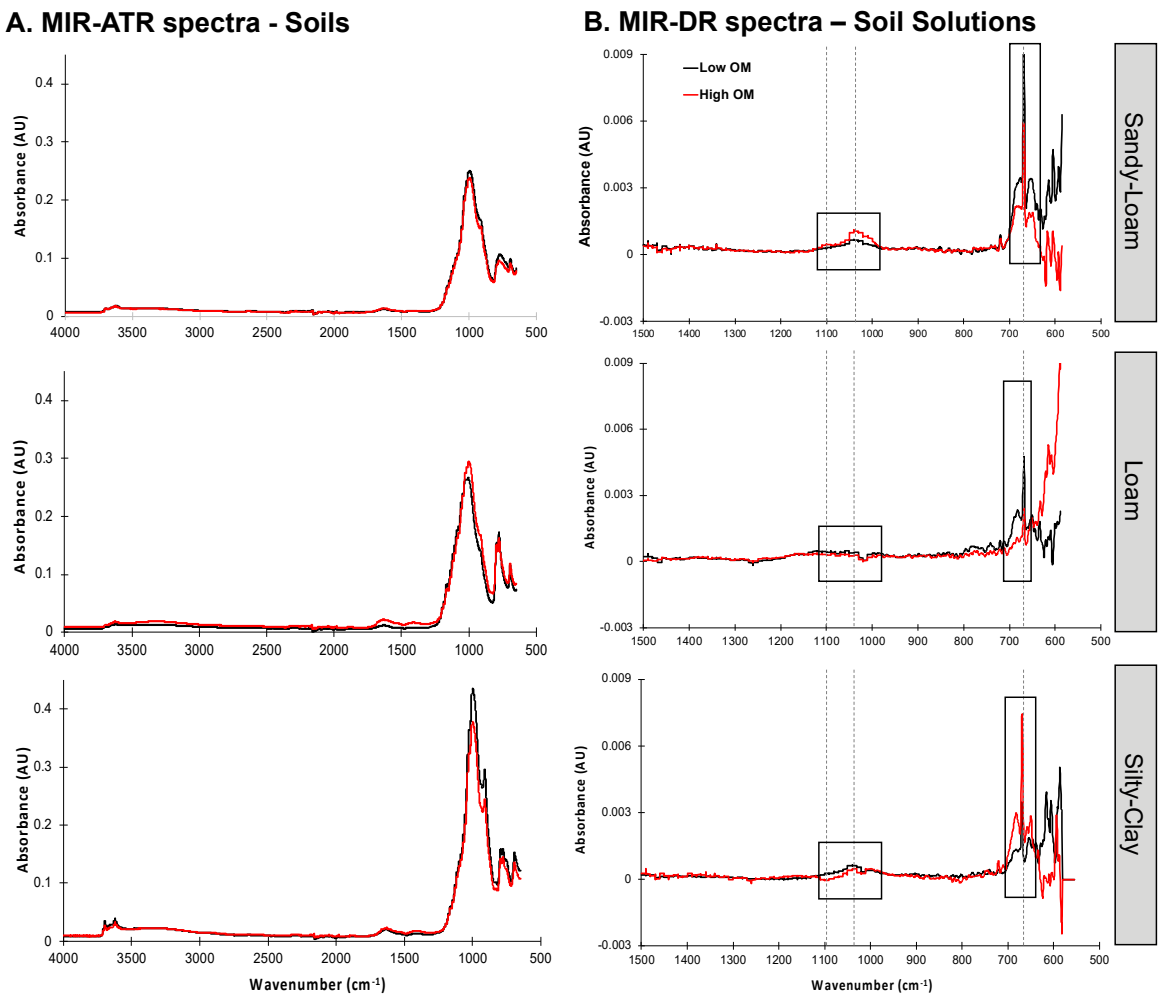

692

693 Figure 3: A) MIR-ATR spectra of the 6 soils. B) MIR-DR spectra of the 6 soil solutions. Each
694 spectrum corresponds to the average of 16 spectra. The vertical grey dotted lines show the
695 position of distinguishable bands of interest as described in the main text: i) Vibrations between
696 700 and 600 cm^{-1} are possibly associated to several elements (ν CO2, ν C-Cl, ν C-Br, ν PO…)
697 due to incomplete correction of the background atmosphere, ii) Vibrations predominantly
698 related to phosphate (e.g. ν PO, ν PO2 -, ν PO3 2-) between 1120 cm^{-1} and 980 cm^{-1}.

699